ISSN 1070-3284, Russian Journal of Coordination Chemistry, 2019, Vol. 45, No. 1, pp. 22–29. © Pleiades Publishing, Ltd., 2019.
Russian Text © O.V. Loseva, T.A. Rodina, A.V. Ivanov, 2019, published in Koordinatsionnaya Khimiya, 2019, Vol. 45, No. 1, pp. 24–31.

# Pseudo-Polymeric Mercury(II) Morpholinedithiocarbamate $[Hg\{S_2CN(CH_2)_4O\}_2]_n$: Supramolecular Structure (a Role of Secondary Hg···S Bonds), $^{13}C$ and $^{15}N$ CP-MAS NMR Spectra, and Thermal Behavior

**O. V. Loseva[a], T. A. Rodina[b], and A. V. Ivanov[a, *]**

[a] *Institute of Geology and Nature Management, Far East Branch, Russian Academy of Sciences, Blagoveshchensk, 675000 Russia*

[b] *Amur State University, Blagoveshchensk, Russia*

**e-mail: alexander.v.ivanov@chemist.com*

Received February 28, 2018; revised April 19, 2018; accepted July 15, 2018

**Abstract**—A new representative of mercury(II) dithiocarbamate complexes, crystalline bis(morpholinedithiocarbamato-*S*,*S*')mercury(II) with the pseudo-1D-polymeric structure, is preparatively synthesized. The structure is characterized by $^{13}C$ and $^{15}N$ MAS NMR spectroscopy and X-ray diffraction analysis (CIF file CCDC no. 1821609). Pairs of symmetric secondary Hg···S bonds (3.400 Å) combine mononuclear $[Hg\{S_2CN(CH_2)_4O\}_2]$ molecules, including planar polygons $[HgS_4]$, into a linear pseudo-polymeric chain. The study of the thermal behavior shows that the two-stage mass loss detected by thermogravimetry is due to the thermal destruction of the complex with the formation of HgS and its subsequent sublimation.

*Keywords:* mercury(II) alkylenedithiocarbamates, structural organization, secondary bonds Hg···S, X-ray diffraction analysis, multinuclear ($^{13}C$, $^{15}N$) MAS NMR spectroscopy, simultaneous thermal analysis

**DOI:** 10.1134/S1070328419010068

## INTRODUCTION

The dithiocarbamate complexes of mercury(II) are convenient precursors for the preparation of film and nanocrystalline mercury sulfides in various thermochemical processes [1–3]. Mercury sulfides are characterized by a small forbidden band gap and, hence, are among promising materials for semiconductor industry in producing ultrasonic sensors, photoelectric converters, infrared detectors, catalysts, and others. In addition, mercury(II) dithiocarbamates are capable of luminescing in both the crystalline state and solution [4, 5] and of efficient chemisorption binding of gold(III) from solutions [6, 7]. Since mercury has a high chemical affinity to sulfur, a number of dithio reagents was proposed for the efficient binding of toxic elemental mercury, which includes oxidation and the formation of stable Hg(II) complexes as individual forms of mercury fixation [8].

Mercury(II) with dialkyl(aryl)dithiocarbamate (symmetrically and nonsymmetrically substituted) and alkylenedithiocarbamate ligands mainly forms molecular complexes of two types: mononuclear $[Hg(S_2CNR_2)_2]$ and binuclear $[Hg_2(S_2CNR_2)_4]$. Each mononuclear complex contains two *S*,*S*'-bidentate-chelating ligands and is characterized by the square-planar (R = $CH_3$ [9], $C_2H_5$ [10, 11], $CH_2CH_2OH$ [12]) or distorted tetrahedral (R = *iso*-$C_3H_7$ [13, 14], *iso*-$C_4H_9$ [15], $C_9H_{10}$ [2], *cyclo*-$C_6H_{11}$ [16]; $R_2$ = *iso*-$C_3H_7$, *cyclo*-$C_6H_{11}$ [15], $C_2H_5$, $C_6H_5$ [17], $CH_2$–$C_4H_3N$–$CH_3$, $CH_2$–$C_6H_5$ [4], $CH_2$–$C_4H_3N$–$CH_3$, $CH_2$–$C_5H_4N$ [5]) geometry of the $[HgS_4]$ chromophore. The binuclear complexes contain two bidentate-chelating and two tridentate-bridging ligands (R = $C_2H_5$ [10], *iso*-$C_3H_7$ [7, 14], $C_4H_9$ [15], $R_2$ = $(CH_2)_4$ [18], $(CH_2)_6$ [19], $CH_3$, $C_6H_5$ [20], $C_2H_5$, *cyclo*-$C_6H_{11}$ [15], *iso*-$C_3H_7$, $CH_2CH_2OH$ [21]). The formally binuclear molecules could be considered as mononuclear fragments coupled due to two additional Hg–S bonds. However, one of the Hg–S bonds in the bridging ligands is substantially weakened, whereas the strength of the bond formed with the mercury atom in the adjacent mononuclear fragment is comparable with that for the terminal ligands. The central eight-membered ring $[Hg_2S_4C_2]$ in the binuclear molecules is stabilized in a chair conformation with the single known exception: $[Hg_2\{S_2CN(C_4H_9)_2\}_4]$ (boat conformation) [15]. Polymorphism in the discussed mercury complexes (for example, three modifications are described for the di-*iso*-propyldithiocarbamate complex: α [13], β [14], and γ [7]) is caused by the participation of mononu-

clear or/and binuclear molecules in the formation of the crystal lattice.

Among the binuclear molecular forms of mercury(II) dithiocarbamates, the $[Hg_2(S_2CNR_2)_4]$ complex ($R_2$ = $CH_2$–$C_{10}H_7$, $CH_2$–$C_5H_4N$) is distinguished by a special dimerization mode: owing to two symmetric Hg–N bonds involving the heterocyclic nitrogen atoms in the peripheral moiety of the ligands [5]. In addition to the mononuclear and binuclear forms, the single trinuclear complex is known for mercury(II): $[Hg_3\{S_2CN(C_9H_{10})\}_6] \cdot N(C_5H_5)$ including the 1,2,3,4-tetrahydroquinolinedithiocarbamate ligand and outer-sphere pyridine molecule [2], as well as the polynuclear cationic complexes, for example, $[Hg_3\{S_2CN(C_2H_5)_2\}_4]^{2+}$ and $[Hg_5\{S_2CN(C_2H_5)_2\}_8]^{2+}$ [22].

Secondary interactions of the nonvalent type (Hg···S, C–H···S, O–H···O, C–H···π) in the crystalline mercury(II) dithiocarbamates result in the formation of diverse supramolecular structures, the systematization of which was discussed in detail [12, 21].

In this work, we synthesized and characterized in detail crystalline bis(morpholinedithiocarbamato-*S*,*S*')mercury(II), $[Hg\{S_2CN(CH_2)_4O\}_2]$ (**I**). This is a new representative of mercury(II) dithiocarbamates with a rare pseudo-1D-polymeric structure, the formation of which provides pair secondary interactions Hg···S between the adjacent molecules. The spectral characteristics, structural organization, and thermal behavior of complex **I** were determined by $^{13}C$ and $^{15}N$ CP-MAS NMR spectroscopy, X-ray diffraction analysis, and simultaneous thermal analysis (STA).

## EXPERIMENTAL

Sodium morpholinedithiocarbamate was synthesized by the reaction of carbon disulfide (Merck) and morpholine (Aldrich) in an alkaline medium [23] and characterized by the $^{13}C$ and $^{15}N$ MAS NMR spectral data. $^{13}C$, $^{15}N$ MAS NMR, δ, ppm: $Na\{S_2CN(CH_2)_4O\} \cdot 2H_2O$: 204.8 ($-S_2CN=$), 67.6, 67.2 ($-OCH_2-$), 54.6, 53.9, 53.5 ($=NCH_2-$); 130.8 (=N–) [24].

**Synthesis of complex I.** Ions $Hg^{2+}$ were precipitated from the aqueous phase with sodium morpholinedithiocarbamate taken in a stoichiometric ratio. A solution containing $Na\{S_2CN(CH_2)_4O\} \cdot 2H_2O$ (0.0841 g, 0.380 mmol) in water (10 mL) was poured to a solution containing $Hg(NO_3)_2 \cdot H_2O$ (Fluka) (0.0651 g, 0.190 mmol) in water (10 mL). To suppress hydrolysis, a solution of mercury(II) nitrate was acidified with nitric acid to pH 2. A fine clotted white precipitate with a yellowish tint was multiply washed with distilled water and dried on a filter. The yield was 99.3%. For diffraction experiment, the powdered complex was dissolved in *N*,*N*-dimethylformamide on heating. The cooling down of the solution was accompanied by the formation of fine needle-like yellowish crystals of complex **I**.

$^{13}C$, $^{15}N$ CP-MAS NMR, δ, ppm: $[Hg\{S_2CN(CH_2)_4O\}_2]_n$: 200.4 (48)* ($-S_2CN=$), 65.8, 65.3 (1 : 1, $-OCH_2-$), 54.4, 53.1 (1 : 1, $=NCH_2-$); 121.9 (60)** (=N–). (* Asymmetric doublet $^{13}C$–$^{14}N$, in Hz; ** spin-spin interaction constant $^3J(^{15}N$–$^{199}Hg)$, in Hz).

**$^{13}C$ and $^{15}N$ CP-MAS CP-NMR spectra** were recorded on an Ascend Aeon spectrometer (Bruker) with a working frequency of 100.64 and 40.56 MHz, respectively, and a superconducting magnet ($B_0$ = 9.4 T) with the closed condensation cycle through an external compressor and Fourier transform. Cross-polarization (CP) from the protons was used, and the proton decoupling effect was applied to suppress $^{13}C$–$^1H$ and $^{15}N$–$^1H$ interactions using the radiofrequency field at the resonance frequency of protons [25]. A sample (~60 mg) was placed in a 4.0-mm ceramic rotor of $ZrO_2$. The magic angle spinning (MAS) of the samples at a frequency of 10000(1) Hz was used to measure $^{13}C$ and $^{15}N$ MAS NMR spectra (the acquisition number was 656 and 20360, duration of proton π/2 pulses was 2.7 and 2.5 μs; the contact time of $^1H$–$^{13}C$ and $^1H$–$^{15}N$ was 3.0 and 3.0 ms, and the interval between pulses was 3.0 and 3.0 s, respectively). Isotropic $^{13}C$ and $^{15}N$ chemical shifts (ppm) are given relative to one of the components of an external standard, which was crystalline adamantane (δ = 38.48 ppm relative to $(CH_3)_4Si$) or crystalline $NH_4Cl$ (δ = 0.0 ppm, or −341 ppm in the absolute scale [26]) with a correction to the drift of the magnetic field strengt the frequency equivalent of which was 0.025 and 0.09 Hz/h, respectively.

**X-ray diffraction analysis** was carried out for needle-like crystals of complex **I** on a Bruker-Nonius X8 Apex CCD diffractometer (Mo$K_\alpha$ radiation, λ = 0.71073 Å, graphite monochromator) at 296(2) K. Data were collected using a standard procedure: φ and ω scan modes of narrow frames. An absorption correction was applied empirically using the SADABS program [27]. The structure was determined by a direct method and refined by least squares (for $F^2$) in the full-matrix anisotropic approximation of non-hydrogen atoms. The positions of hydrogen atoms were calculated geometrically and included into the refinement in the riding model. The calculations of structure determination and refinement were performed using the SHELXTL program package [27]. The main crystallographic data and the structure refinement results for complex **I** are presented in Table 1. Selected bond lengths and bond angles are given in Table 2.

The coordinates of atoms, bond lengths, and angles were deposited with the Cambridge Crystallographic Data Centre (CIF file CCDC no. 1821609; deposit@ccdc.cam.ac.uk or http://www.ccdc.cam.ac.uk).

**Table 1.** Crystallographic data and the experimental and structure refinement parameters for complex **I**

| Parameter | Value |
|---|---|
| Empirical formula | $C_{10}H_{16}N_2O_2S_4Hg$ |
| *FW* | 525.08 |
| Crystal system | Monoclinic |
| Space group | $P2_1/n$ |
| *a*, Å | 4.2660(7) |
| *b*, Å | 11.616(2) |
| *c*, Å | 14.999(3) |
| α, deg | 90.00 |
| β, deg | 94.067(5) |
| γ, deg | 90.00 |
| *V*, Å$^3$ | 741.4(2) |
| *Z* | 2 |
| $\rho_{calcd}$, g/cm$^3$ | 2.352 |
| μ, mm$^{-1}$ | 10.941 |
| *F*(000) | 500 |
| Crystal size, mm | 0.12 × 0.02 × 0.02 |
| Range of data collection over θ, deg | 2.22–27.61 |
| Ranges of reflection indices | $-5 \le h \le 5$, $-15 \le k \le 15$, $-1 \le l \le 19$ |
| Measured reflections | 5366 |
| Independent reflections ($R_{int}$) | 1668 (0.0489) |
| Reflections with $I > 2\sigma(I)$ | 1229 |
| Refinement variables | 89 |
| GOOF | 1.012 |
| *R* factors for $F^2 > 2\sigma(F^2)$ | $R_1 = 0.0347$, $wR_2 = 0.0666$ |
| *R* factors for all reflections | $R_1 = 0.0590$, $wR_2 = 0.0718$ |
| Residual electron density (min/max), e/Å$^3$ | −1.065/1.320 |

**Thermal behavior of complex I** was studied by the STA method on a STA 449C Jupiter instrument (NETZSCH) in corundum crucibles under caps with a hole providing a vapor pressure of 1 atm upon the thermal decomposition of the sample. The heating rate was 5°C/min to 600°C under argon. The sample weight was 2.972–7.295 mg. The accuracy of the temperature measurement was ±0.7°C, and that of the mass change was $\pm 1 \times 10^{-4}$ mg. The correction file and temperature and sensitivity calibrations for the specified temperature program and heating rate were used when recording curves of thermogravimetry (TG) and differential scanning calorimetry (DSC). The melting point of complex **I** was determined independently on a PTP(M) instrument (OAO Khimlaborpribor).

## RESULTS AND DISCUSSION

The $^{13}C$ resonance signals in the MAS NMR spectrum of a polycrystalline sample of complex **I** were assigned to the $=NC(S)S-$, $-OCH_2-$, and $=NCH_2-$ groups (Fig. 1*a*). The pairs of signals of equal intensity from each of two last groups indicate their structural nonequivalence in the $-N(CH_2-CH_2)_2O$ cyclic fragment of the ligand. The carbon atom in the dithiocarbamate group is directly bound to the nitrogen atom by the short N–C(S)S bond characterized by a significant contribution of double bonding. Therefore, the $=NC(S)S-$ group is presented in the spectrum by the asymmetric doublet with an intensity ratio of 1 : 2 (Fig. 1a) due to the dipole–dipole interaction of the $^{13}C$ nucleus with the $^{14}N$ quadrupole nucleus ($I = 1$) [28, 29]. The single $^{15}N$ resonance signal in the MAS NMR spectrum (Fig. 1*b*) indicates that the MfDtc

**Table 2.** Selected bond lengths (*d*) and bond (ω) and torsion (φ) angles in the structure of complex **I***

| Bond | *d*, Å | Bond | *d*, Å |
|---|---|---|---|
| Hg(1)–S(1) | 2.4028(16) | N(1)–C(2) | 1.470(8) |
| Hg(1)–S(2) | 2.9041(18) | N(1)–C(5) | 1.462(7) |
| Hg(1)···S(1)[b] | 3.400(2) | O(1)–C(3) | 1.425(8) |
| S(1)–C(1) | 1.763(6) | O(1)–C(4) | 1.417(8) |
| S(2)–C(1) | 1.681(7) | C(2)–C(3) | 1.512(8) |
| N(1)–C(1) | 1.335(7) | C(4)–C(5) | 1.521(7) |
| Angle | ω, deg | Angle | ω, deg |
| S(1)Hg(1)S(2) | 67.45(5) | Hg(1)S(2)C(1) | 78.9(2) |
| S(1)Hg(1)S(2)[a] | 112.55(5) | S(1)C(1)S(2) | 119.5(3) |
| S(1)[a]Hg(1)S(1)[b] | 86.96(5) | S(1)C(1)N(1) | 116.8(5) |
| S(1)Hg(1)S(1)[b] | 93.04(5) | S(2)C(1)N(1) | 123.7(5) |
| S(2)Hg(1)S(1)[b] | 94.77(5) | C(1)N(1)C(2) | 124.0(5) |
| S(2)[a]Hg(1)S(1)[b] | 85.23(5) | C(1)N(1)C(5) | 121.8(5) |
| Hg(1)S(1)C(1) | 93.4(2) | C(2)N(1)C(5) | 113.3(5) |
| Angle | φ, deg | Angle | φ, deg |
| Hg(1)S(1)S(2)C(1) | 170.2(4) | S(1)C(1)N(1)C(5) | 171.9(4) |
| S(1)Hg(1)C(1)S(2) | 171.8(4) | S(2)C(1)N(1)C(2) | −176.7(5) |
| S(1)C(1)N(1)C(2) | 3.3(8) | S(2)C(1)N(1)C(5) | −8.1(8) |

* Symmetry transforms: [a] $1-x, 1-y, -z$; [b] $x-1, y, z$.

ligands in complex **I** are equivalent (and, therefore, have the same structural function), which is consistent with the $^{13}C$ NMR data. The signal discussed is characterized by broadening from two sides due to overlapping with two satellite lines symmetrically arranged relatively to the central $^{15}N$ signal with the intensity ratio close to 1 : 10 : 1 (Fig. 1*b*). This is rather typical of the mercury(II) dithiocarbamates [19], since natural mercury includes nuclide $^{199}Hg$ ($\mu = 0.5058852\ \mu_N$, $I = 1/2$). Therefore, the multiplet structure of the resonance $^{15}N$ signal appears due to the spin-spin interaction between the $^{15}N$ and $^{199}Hg$ nuclei with the constant $^3J(^{15}N–^{199}Hg)$ equal to 60 Hz. The natural abundance of nuclide $^{199}Hg$ (16.87 at %) determines the

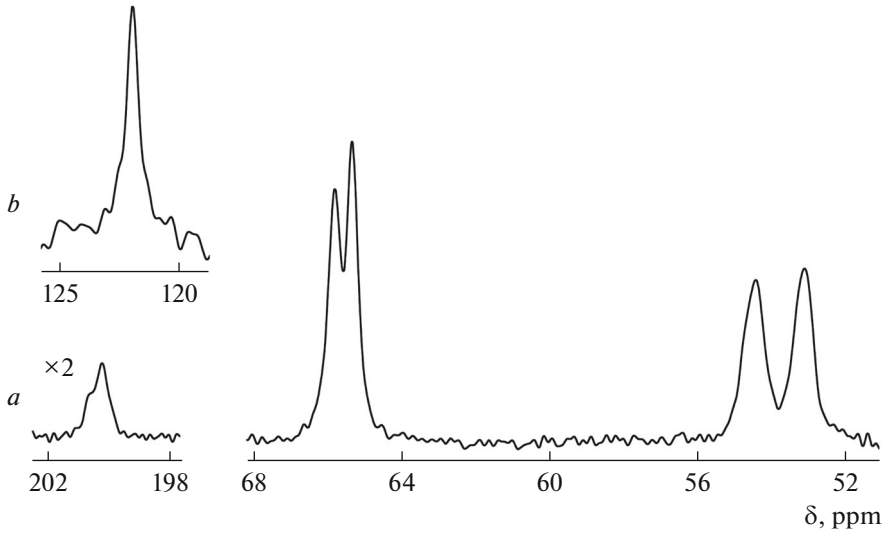


**Fig. 1.** (*a*) $^{13}C$ and (*b*) $^{15}N$ MAS NMR spectra of complex **I**. The spinning frequency of the sample is 10 kHz, and the acquisition number is (*a*) 656 and (*b*) 20360.

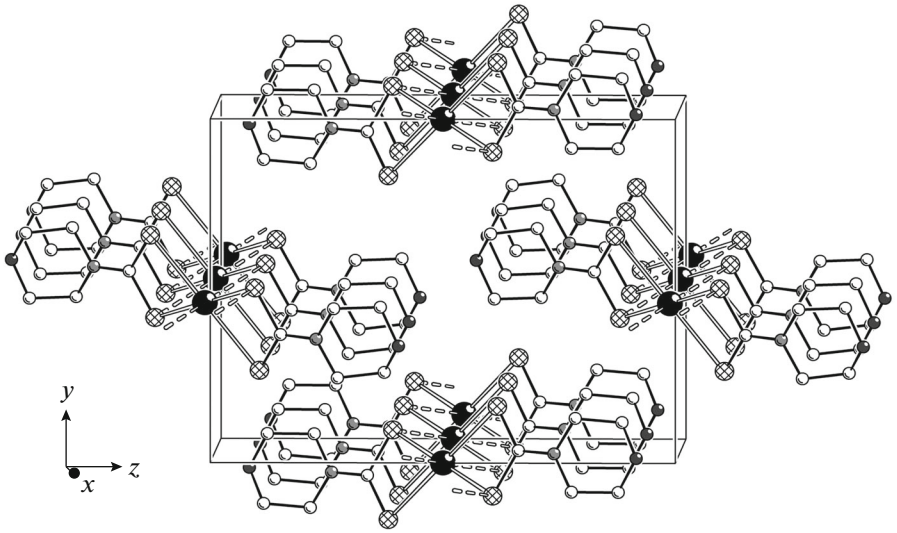


**Fig. 2.** Packing of structural units in the crystal of complex **I** (projection on the *yz* plane).

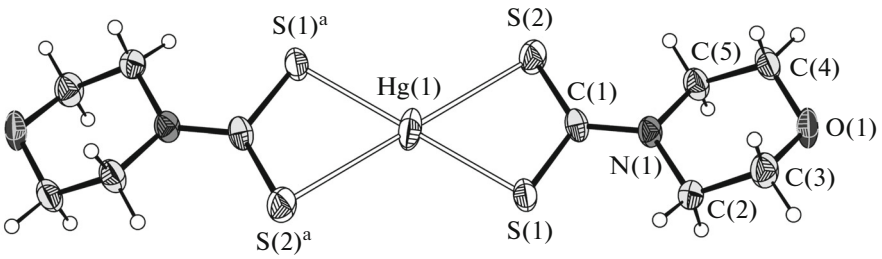


**Fig. 3.** Molecular structure of $[Hg\{S_2CN(CH_2)_4O\}_2]$ (ellipsoids of 50% probability).

contribution of equidistant satellite signals to the total intensity of the $^{15}N$ signal.

The structural organization of complex **I** was determined by X-ray diffraction analysis. The unit cell contains two formula units (for the packing of structural units, see Fig. 2). The structural unit of compound **I** is the centrosymmetric molecule $[Hg\{S_2CN(CH_2)_4O\}_2]$ (Fig. 3) in which mercury(II) coordinates two *S*,*S*'-anisobidentate MfDtc ligands to form a rectangular chelate node $[HgS_4]$. The S(1)···S(2) intraligand distances (2.976 Å) are much shorter than the interligand S(1)···S(2)$^a$ distances (4.423 Å). The rigidly planar configuration of the latter (the diagonal bond angles S(1)Hg(1)S(1)$^a$ and S(2)Hg(1)S(2)$^a$ are 180°) is caused by the outer-orbital $sp^2d$-hybridization state of the central mercury atom. The Hg–S bonds are substantially nonequivalent: Hg(1)–S(1) 2.4028 and Hg(1)–S(2) 2.9041 Å (Table 2). However, the first bond is consistent with the sum of covalent and empirical covalent radii of sulfur and mercury atoms (2.37 and 2.51 Å [30]), whereas the length of the second bond significantly exceeds these values. Nevertheless, this interatomic distance is considerably less than the sum of the van der Waals radii (3.35 Å [30]), which makes it possible to consider that the second bond is also covalent although substantially weakened. The diagonal arrangement of the uniform Hg–S bonds determines the long (S(2)–S(2)$^a$ 5.808 Å) and short (S(1)–S(1)$^a$ 4.806 Å) axes of the orthorhombic distortion of the $[HgS_4]$ coordination tetragon and the deviation of the angles formed by the sulfur atoms from the right angle: S(1)S(2)S(1)$^a$ 78.34° and S(2)S(1)S(2)$^a$ 101.66°.

The bidentate coordination mode of the MfDtc ligands results in the formation of two metallocycles $[HgS_2C]$ (unified by the common mercury atom), whose small sizes agree with the interatomic distances Hg–C (3.064 Å) and S–S (2.976 Å). The mutual arrangement of the atoms in the cycles somewhat deviates from the coplanar one, which is indicated by the values of torsion angles Hg(1)S(1)S(2)C(1) (170.2°) and S(1)Hg(1)C(1)S(2) (171.8°) (Table 2). The strength of the N–C(S)S bonds is appreciably higher than that of N–$CH_2$ (Table 2). The bond angles at the carbon and nitrogen atoms are close to 120° due to the contribution of double bonding to the formally ordi-

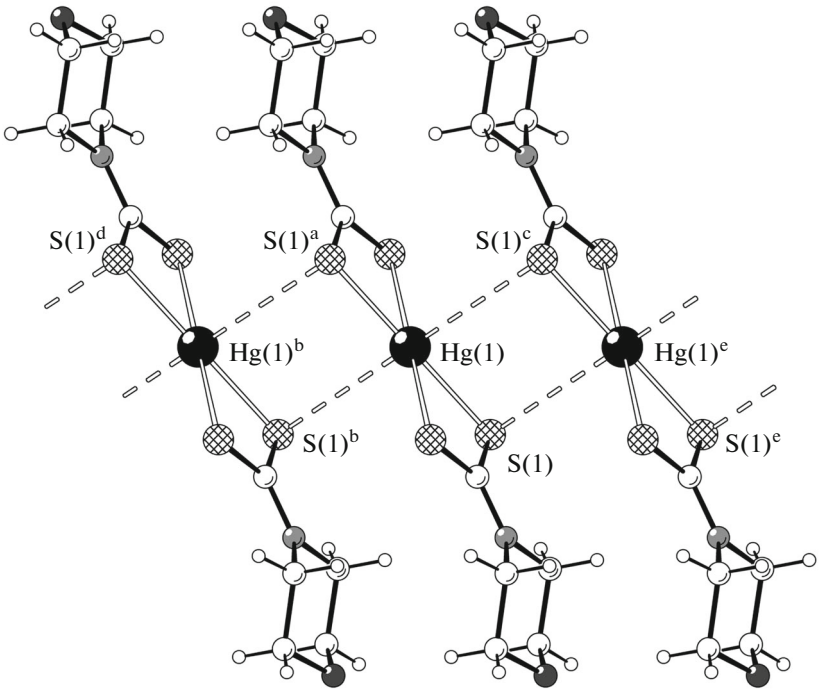


**Fig. 4.** Fragment of the pseudopolymeric chain of complex **I** oriented along the crystallographic axis *x*; secondary interactions Hg···S are shown by dashed lines. Symmetry transforms: [a] $1-x, 1-y, -z$; [b] $x-1, y, z$; [c] $2-x, 1-y, -z$; [d] $-x, 1-y, -z$; [e] $1+x, y, z$.

nary N–C(S)S bond (owing to the admixing of the $sp^2$- to $sp^3$-hybridization state of the nitrogen and carbon atoms). Small deviations (by 3.3° and 8.1°) of the SCNC torsion angles from 0° or 180° indicate the predominantly planar geometry of the $C_2NC(S)S$ groups in the MfDtc ligands (Table 2). The six-membered heterocycles $-N(CH_2)_4O$ are stabilized in the chair conformation and are located on opposite sides relative to the plane of the $[HgS_4]$ chelate node (*trans* orientation).

The supramolecular structure of complex **I** is formed due to pair secondary interactions of the nonvalent type involving the Hg(1) atoms and diagonally oriented S(1) atoms less strongly bound to the central mercury atom (Fig. 4). Therefore, each $[Hg\{S_2CN\text{-}(CH_2)_4O\}_2]$ molecule forms two pairs of secondary bonds with the nearest neighbors to form linear pseudo-polymeric chains $[Hg\{S_2CN\text{-}(CH_2)_4O\}_2]_n$ (interatomic distance Hg–Hg 4.266 Å) oriented along the crystallographic *x* axis. The length of the pair secondary bonds Hg(1)···S(1)[b] and Hg(1)···S(1)[c] (3.400 Å) is close to the sum of the van der Waals radii of mercury and sulfur atoms: 3.35 Å [30]. The mercury atom completes its polyhedron to a distorted octahedron $[HgS_6]$ (angle S(1)[b]Hg(1)S(1)[c] 180°) due to additional secondary Hg···S bonds in the axial positions. Thus, among numerous mercury(II) dithiocarbamates known to the present time, mononuclear compound **I** is characterized by a combination of two structural features: the planar polygon $[HgS_4]$ and self-assembling of the pseudo-polymeric chain, which has been found only for two complexes more: $[Hg(S_2CNR_2)_2]_n$ (R = $C_2H_5$ [10, 11] and $CH_2CH_2OH$ [12]).

The thermal behavior of complex **I** was studied by the STA method with the simultaneous detection of TG and DSC curves. The compound is thermally stable to ~210°C. In the TG curve, two main mass loss steps are determined by the ranges 210–315°C and 315–405°C (Fig. 5, curve *a*). The first, steeply descending region is divided into two sections by the inflection point at 291.0°C. The mass loss before the inflection point (26.76%) suggests that the initial stage of thermolysis of complex **I** is related to the elimination of the alkoxyl fragments of the $(=CHCH_2)_2O$ ligands (calcd. 26.70%) to which the formation of an intermediate compound $[Hg(S_2CNH_2)_2]$ can correspond. The further temperature increase is accompanied by an increase in the thermolysis rate resulting in the liberation of HgS [7, 20]. It is important that the mass loss after the inflection point, which is equal to 47.32%, significantly exceeds the calculated value (28.99%).

The second, a more flat step of the TG curve (315–405°C) is related to HgS sublimation [7, 20]. However, the mass loss detected in this step (21.89%) is underes-

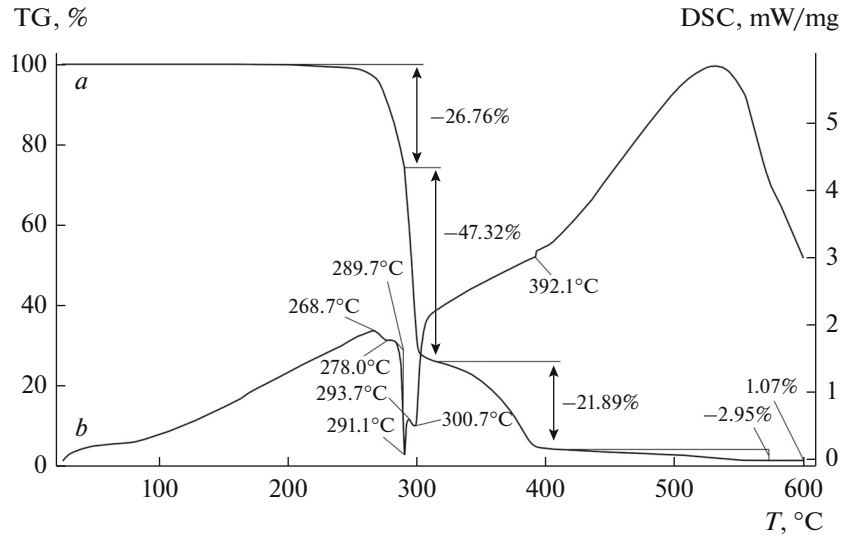


**Fig. 5.** (*a*) TG and (*b*) DSC curves for complex **I**.

timated more than twice compared to the calculated value for HgS (44.31%). Taking into account the overestimation of the mass loss in the first step of the TG curve (after 291°C), one can conclude that a significant portion of HgS (18.33%) sublimes before the onset of the second step and is superimposed on the first stage of thermolysis. The earlier study of the thermal behavior of a compact powder of HgS made it possible to establish the onset of its sublimation already at 225°C [7]. The region of the final desorption (2.95%) of volatile thermolysis products is presented in the TG curve from 405°C to the stabilization of the crucible weight at 570°C. Traces of a light gray coating (1.07%) are observed on the bottom of the crucible after the end of thermolysis at 600°C, which can be associated with the formation of elemental carbon.

The region of the DSC curve projected onto the first step of the TG curve contains three thermal effects (Fig. 5, curve *b*). The first, weakly pronounced endothermic effect with an extreme at 278.0°C (extrapolated temperature 268.7°C) shows the initial step of mass loss. The second endothermic effect at 291.1°C should be attributed to the melting of the substance during decomposition of the sample with decomposition was determined independently in a glass capillary to occur at 289–290°C. The third endothermic effect at 300.7°C with an extrapolated temperature of 293.7°C corresponds to the thermolysis of the sample after the inflection point. A weakly pronounced thermal effect at 392.1°C corresponds to the completion of HgS sublimation (the second step of mass loss).

## ACKNOWLEDGMENTS

The authors are grateful to Prof. O.N. Antsutkin and Dr. V. Gowda (Luleå University of Technology, Sweden) for the kindly presented possibility and help in recording $^{13}C$ and $^{15}N$ MAS NMR spectra.

## REFERENCES

1. Dar, S.H., Thirumaran, S., and Selvanayagam, S., *Polyhedron*, 2015, vol. 96, p. 16.
2. Srinivasan, N., Thirumaran, S., and Ciattini, S., *RSC Adv.*, 2014, vol. 4, no. 44, p. 22971.
3. Onwudiwe, D.C. and Ajibade, P.A., *Mater. Lett.*, 2011, vol. 65, nos. 21–22, p. 3258.
4. Yadav, M.K., Rajput, G., Gupta, A.N., et al., *Inorg. Chim. Acta*, 2014, vol. 421, p. 210.
5. Rajput, G., Yadav, M.K., Thakur, T.S., et al., *Polyhedron*, 2014, vol. 69, p. 225.
6. Loseva, O.V., Rodina, T.A., Smolentsev, A.I., and Ivanov, A.V., *Russ. J. Coord. Chem.*, 2016, vol. 42, no. 11, p. 719. doi 10.1134/S1070328416110063
7. Loseva, O.V., Rodina, T.A., Smolentsev, A.I., and Ivanov, A.V., *Polyhedron*, 2017, vol. 134, p. 238.
8. Mercuri, M.L., Serpe, A., Marchio, L., et al., *Inorg. Chem. Comm.*, 2014, vol. 39, p. 47.
9. Cox, M.J. and Tiekink, E.R.T., *Z. Kristallogr.*, 1997, vol. 212, no. 7, p. 542.
10. Iwasaki, H., *Acta Crystallogr., Sect. B: Struct. Crystallogr. Cryst. Chem.*, 1973, vol. 29, no. 10, p. 2115.
11. Healy, P.C. and White, A.H., *J. Chem. Soc., Dalton Trans.*, 1973, no. 3, p. 284.
12. Howie, R.A., Tiekink, E.R.T., Wardell, J.L., and Wardell, S.M.S.V., *J. Chem. Crystallogr.*, 2009, vol. 39, no. 4, p. 293.
13. Ito, M. and Iwasaki, H., *Acta Crystallogr., Sect. B: Struct. Crystallogr. Cryst. Chem.*, 1979, vol. 35, no. 11, p. 2720.

14. Iwasaki, H., Ito, M., and Kobayashi, K., *Chem. Lett.*, 1978, vol. 7, p. 1399.

15. Cox, M.J. and Tiekink, E.R.T., *Z. Kristallogr.*, 1999, vol. 214, no. 9, p. 571.

16. Cox, M.J. and Tiekink, E.R.T., *Main Group Met. Chem.*, 2000, vol. 23, no. 12, p. 793.

17. Onwudiwe, D.C. and Ajibade, P.A., *J. Chem. Crystallogr.*, 2011, vol. 41, no. 7, p. 980.

18. Altaf, M., Stoeckli-Evans, H., Batool, S.S., et al., *J. Coord. Chem.*, 2010, vol. 63, no. 7, p. 1176.

19. Ivanov, A.V., Korneeva, E.V., Bukvetskii, B.V., et al., *Russ. J. Coord. Chem.*, 2008, vol. 34, no. 1, p. p. 59. doi 10.1134/S1070328408010107

20. Onwudiwe, D.C. and Ajibade, P.A., Int. *J. Mol. Sci.*, 2011, vol. 12, no. 3, p. 1964.

21. Jotani, M.M., Tan, Y.S., and Tiekink, E.R.T., *Z. Kristallogr.*, 2016, vol. 231, no. 7, p. 403.

22. Bond, A.M., Colton, R., Hollenkamp, A.F., et al., *J. Am. Chem. Soc.*, 1987, vol. 109, no. 7, p. 1969.

23. Byr'ko, V.M., *Ditiokarbamaty* (Dithiocarbamates), Moscow: Nauka, 1984.

24. Ivanov, A.V., Ivakhnenko, E.V., Gerasimenko, A.V., and Forsling, W., *Russ. J. Inorg. Chem.*, 2003, vol. 48, no. 1, p. 45.

25. Pines, A., Gibby, M.G., and Waugh, J.S., *J. Chem. Phys.*, 1972, vol. 56, no. 4, p. 1776.

26. Ratcliffe, C.I., Ripmeester, J.A., and Tse, J.S., *Chem. Phys. Lett.*, 1983, vol. 99, no. 2, p. 177.

27. *APEX2 (version 1.08), SAINT (version 7.03), SADABS (version 2.11), SHELXTL (version 6.12)*, Madison: Bruker AXS Inc., 2004.

28. Hexem, J.G., Frey, M.H., and Opella, S.J., *J. Chem. Phys.*, 1982, vol. 77, no. 7, p. 3847.

29. Harris, R.K., Jonsen, P., and Packer, K.J., *Magn. Res. Chem.*, 1985, vol. 23, no. 7, p. 565.

30. Winter, M., WebElements Periodic Table of the Elements, http://www.webelements.com. Accessed January, 2010.

*Translated by E. Yablonskaya*